ROYAL SOCIETY
OF CHEMISTRY

PAPER

Check for updates

An inorganic water-based paint for high-durability passive radiative cooling†

Siyuan Li,[a] Xianglin Zhang,[d] Yanfei Yang,[a] Xin Li,[a] Hongbo Xu, [iD][a] Juyan Zhao,*[d] Lorenzo Pattelli, [iD] *[c] Lei Pan,*[a] Jiupeng Zhao [iD][a] and Yao Li*[b]

Due to the extreme reflectivity requirements of radiative cooling coatings, these materials often employ ceramic nanoparticles such as TiO_2 due to their high refractive index and scattering efficiency. However, the bandgap of TiO_2 (3.2 eV) is lower than the energy of the most energetic solar light, leading to significant absorption in the UV range (0.25–0.4 μm) and subsequent oxidation aging and yellowing of particles and/or organic binders. To overcome the conflict between high reflective efficiency and UV durability, formulations using high-bandgap materials can be used despite their lower refractive index. In this work, we describe an optimized PRC-Al_2O_3 coating by adjusting the ratio of low refractive index alumina particles to sodium methylsilicate adhesive. The PRC-Al_2O_3 exhibits a high solar reflectance above 0.96 and a high mid-infrared emissivity of 0.92, enabling it to achieve a maximum theoretical cooling power of 109 W m^{-2}. Following continuous UV irradiation with a power of 0.7 kW m^{-2} for 72 hours, only a marginal 0.2% decline in solar reflectance occurred compared to the unaged coatings. The resulting anti-aging cooling paint is scalable and can be spray-coated onto outdoor structures and containers, providing durable radiative cooling towards real-world applications.

1. Introduction

With the exacerbation of global warming and its associated environmental challenges, there is an imperative to investigate sustainable cooling technologies.[1–3] Passive radiative coolers (PRCs) can achieve sub-ambient cooling owing to their extreme solar reflectance and radiative heat dissipation *via* atmospheric windows.[4,5] These technologies hold promise for diverse applications in the building sector,[6–8] personal thermal management,[9,10] photovoltaic modules,[11,12] and more.[13] Due to the large scale of these applications, highly scalable methods such as spraying are attracting significant research efforts. Many polymer coatings have been prepared and have produced good radiation cooling effects.[14–16] However, exposure to ultraviolet (UV) radiation induces a yellowish coloration in coatings containing polymers,

thereby diminishing their solar reflectivity and mechanical durability, presenting a challenge for practical application.[17] On the other hand, inorganic adhesives exhibit remarkable UV resistance while possessing a high infrared emittance attributed to the molecular bond resonances within the atmospheric transparency window,[18] but have received surprisingly little attention up to now.

Notably, the inclusion of inorganic scatterers in the coating may also accelerate UV-induced degradation. Achieving high reflectivity in coatings typically involves the utilization of high refractive index scatterers ($n > 2.5$) like TiO_2.[19,20] However, in accordance with Moss' law, high refractive index scatterers often possess a low bandgap, leading to significant absorption in the ultraviolet spectrum.[21,22] Besides, under UV irradiation, hydrogen atoms in water molecules or organic compounds adsorbed on the surface of TiO_2 particles may oxidize and penetrate into the TiO_2 lattice, resulting in increased light absorption and yellowing of TiO_2 particles and/or organic binders.[23–25]

Recently, researchers have proposed using high concentrations of low-refractive-index particles (*e.g.*, $BaSO_4$[26] and $CaCO_3$[27]) within a polymer matrix to achieve a continuous cooling effect during both daytime and nighttime. These findings indicate significant potential for achieving daytime passive radiative cooling in a scalable manner by utilizing particles that effectively scatter the full spectrum of solar irradiation. However, the patterned surface structures and high particle concentrations present challenges that hinder practical applications, requiring the use of volatile organic solvents. Moreover, baryte is listed among the critical raw materials, and $CaCO_3$ is easily

[a] MIIT Key Laboratory of Critical Materials Technology for New Energy Conversion and Storage, School of Chemistry and Chemical Engineering, Harbin Institute of Technology, Harbin 150001, China. E-mail: panlei@hit.edu.cn

[b] Center for Composite Materials and Structure, Harbin Institute of Technology, Harbin 150001, China. E-mail: liyao@hit.edu.cn

[c] Istituto Nazionale di Ricerca Metrologica (INRiM), Turin 10135, Italy. E-mail: l.pattelli@inrim.it

[d] National Key Laboratory of Science and Technology on Test Physics and Numerical Mathematics, Beijing, 100076, China. E-mail: zhaojuyan1980@sohu.com

† Electronic supplementary information (ESI) available. See DOI: https://doi.org/10.1039/d4tc04108a

This journal is © The Royal Society of Chemistry 2025

J. Mater. Chem. C, 2025, **13**, 4137–4144 | **4137**

dissolved by chemical agents. More abundant and durable alternatives are represented by SiO_2[28,29] and Al_2O_3,[30–32] which have also been used both as scatterers in particle–polymer composite coolers, and as monolithic materials upon sintering. Such high-temperature processes, however, limit the scalable application of these materials and increase the cost and carbon footprint associated with their fabrication significantly. There is a strong need to develop high-performance radiative cooling materials that allow for easy fabrication and demonstrate good applicability. Relevant examples exist in nature of organisms which can achieve high opacity using only low-index materials, suggesting that similar results could be achieved by carefully tuning the solid volume fraction and morphology of the coating.[33]

Hence, in this study, we selected Al_2O_3 as the scatterer material, owing to its large bandgap, exceptional stability, chemical and thermal resistance, low cost, vanishing absorption in the solar range, moderate refractive index, and high thermal emissivity. A wet spray coating (PRC-Al_2O_3) was prepared by mixing a composite of Al_2O_3 and methylated sodium silicate adhesive with water. Compared to other paint-like materials, the coating is environmentally friendly, without volatile organic solvents, is non-toxic, and exhibits significant UV aging resistance and favourable hydrophobic characteristics upon surface treatment with perfluorodecyltriethoxysilane solution.

2. Methods

2.1. Materials

Four types of alumina powders (99.9%) with different particle sizes were used in this research, which we refer to as ZY-1, ZY-2, ZY-3 and ZY-4. ZY-1, ZY-2, and ZY-3 were procured from Qinghe County Huiguang Metal Materials Co., Ltd, and ZY-4 was procured from Zhongzhi New Material Co., Ltd. Sodium methylsilicate was obtained from Shandong Guohua Chemical Co., Ltd. $1H,1H,2H,2H$-perfluorodecyltriethoxysilane (PFDTS) (96%) was acquired from Aladdin Chemical Reagent Co., Ltd, China. Commercial inorganic coatings (CIC) were purchased from Huifu Materials Co., Ltd, mainly composed of titanium dioxide and silicates. The substrates included aluminium plate, glass, and anodized aluminium plate (black), all sourced from Guangdong Dixuan Aluminum. Ethanol, n-hexane, and the acid–base reagent raw materials were purchased from China National Pharmaceutical Group Chemical Reagent Co., Ltd. All purchased reagents were used directly without further purification.

2.2. Coating preparation

The radiation-cooled coating is obtained by combining alumina and sodium methylsilicate in a specific ratio, stirring for 30 minutes to ensure uniform mixing (Fig. 1). Next, the paint is evenly applied onto the substrate and allowed to dry for 24 hours. Lastly, an additional coating of sodium methylsilicate is sprayed onto the cured surface and air dried for 12 hours to create a continuous barrier and avoid contamination. Optionally, the coating can be then immersed or sprayed with 2% n-hexane PFDTS solution, rinsed with ethanol and cured at room temperature for 24 hours, to endow the coating with hydrophobic properties.

2.3. Characterization

Finite-difference time-domain (FDTD) numerical simulations were conducted to determine the scattering efficiency of aluminium oxide particles of varying sizes in air. The microstructure of the coating was characterized by scanning electron microscopy (SEM, SIGMA 300, ZEISS, Germany) at a voltage of 10 kV and microscope (DM4 P, Leica, Germany). The diameter distribution was analysed based on the SEM images using Nano Measure 1.2. Coating reflectivity was assessed using an ultraviolet-visible near infrared (UV-vis-NIR) spectrophotometer (Lambda-1050+, PerkinElmer, USA).

Humidity and wind speed were measured using a hygrometer and an anemometer, respectively. Real-time temperature data both inside the box and outside it were recorded using a data logger thermometer equipped with thermocouples (EX4000, Yili (Shenzhen) Technology Co., Ltd, China). To assess the ambient cooling performance of coating in Harbin, China (45°43′49″N, 126°38′11″E, Altitude 128 m) under direct sunlight, a custom-made device was utilized. This device comprised thermocouples, a temperature signal conversion module, and an aluminium foil-coated polystyrene foam box covered with PE films, featuring three identical rectangular pockets (6 cm × 8 cm × 3 cm) for holding test samples (4 cm × 4 cm) and thermocouples. Placed on a shelf above the roof, it minimized ground heat convection. Additionally, simulated sunlight irradiation experiments were conducted indoors using a xenon lamp (PLS-ILS, Perfect light Technology Co., Ltd, China).

UV accelerated aging experiments were conducted using a UV accelerated aging tester (UV600, SANWOOD, China), with temperature, humidity, and other experimental conditions maintained appropriately and consistently throughout the test. The contact angle tester (JY-82A, Chengde Dingsheng experimental machine testing equipment Co., Ltd, China) was used to take the images of the water contact angle (CA) of the material. Coating adhesion was tested according to ISO 16276-2:2007 standards, and a universal tensile testing machine (AGXplus, Shimadzu, Japan) was used to evaluate the bond strength between the coating and the substrate.
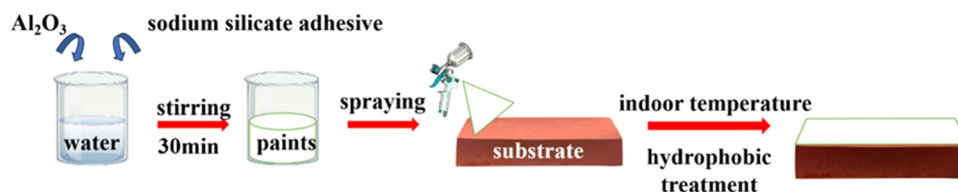

Fig. 1 Coating preparation process.

4138 | *J. Mater. Chem. C*, 2025, **13**, 4137–4144

This journal is © The Royal Society of Chemistry 2025

3. Results and discussion

3.1. Optimization of scatterer size

In order to ensure the reflectivity of the coating in the entire solar spectrum while mitigating UV aging, a scatterer with a moderate refractive index must be selected. Alumina, as depicted in Fig. 2a, exhibits a refractive index of 1.75 across the solar spectrum combined with a vanishing extinction coefficient, resulting in minimal UV absorption and facilitating the preparation of highly reflective coatings.[34]

The size of the scatterer significantly influences the coating's reflectivity, underscoring the importance of selecting the appropriate alumina particle size. A numerical investigation of the scattering capabilities of Al_2O_3 (depicted in Fig. 2b) was conducted using Mie theory, comparing it against spheres of equal radius. Fig. 2b illustrates the scattering efficiency of alumina with diameters ranging from 0.5 to 3 μm, indicating a high scattering efficiency for scatterer sizes comparable to

visible wavelengths. This finding suggests that a wide size distribution is advantageous for coatings to effectively scatter light within the whole solar spectrum, necessitating the combination of multiple scatterers with different particle sizes.

Alumina powder (designated as ZY-2) meeting the required particle size distribution was selected to be mixed with sodium methylsilicate at a ratio of 4 : 1 to prepare a coating, labelled as PRC-2. Scanning electron microscopy images of ZY-2 and its particle size distribution statistics are presented in Fig. 2c and d, respectively, with diameters ranging from 0 to 4 μm. Additionally, three other powders with different diameters (ZY-1, ZY-3, ZY-4) were employed to prepare coatings (PRC-1, PRC-3, PRC-4, respectively) for comparative analysis. As shown in Fig. S1 (ESI†), the particle sizes predominantly fall within the ranges of 0.05–0.35 μm, 0–4.5 μm, and 1.5–15 μm, respectively.

Reflectance profiles of four coatings are depicted in Fig. 2e, while the integrated solar reflectance (R_s) is illustrated in Fig. 2f, quantified as 91.8%, 95.2%, 94.5%, and 92.1%,
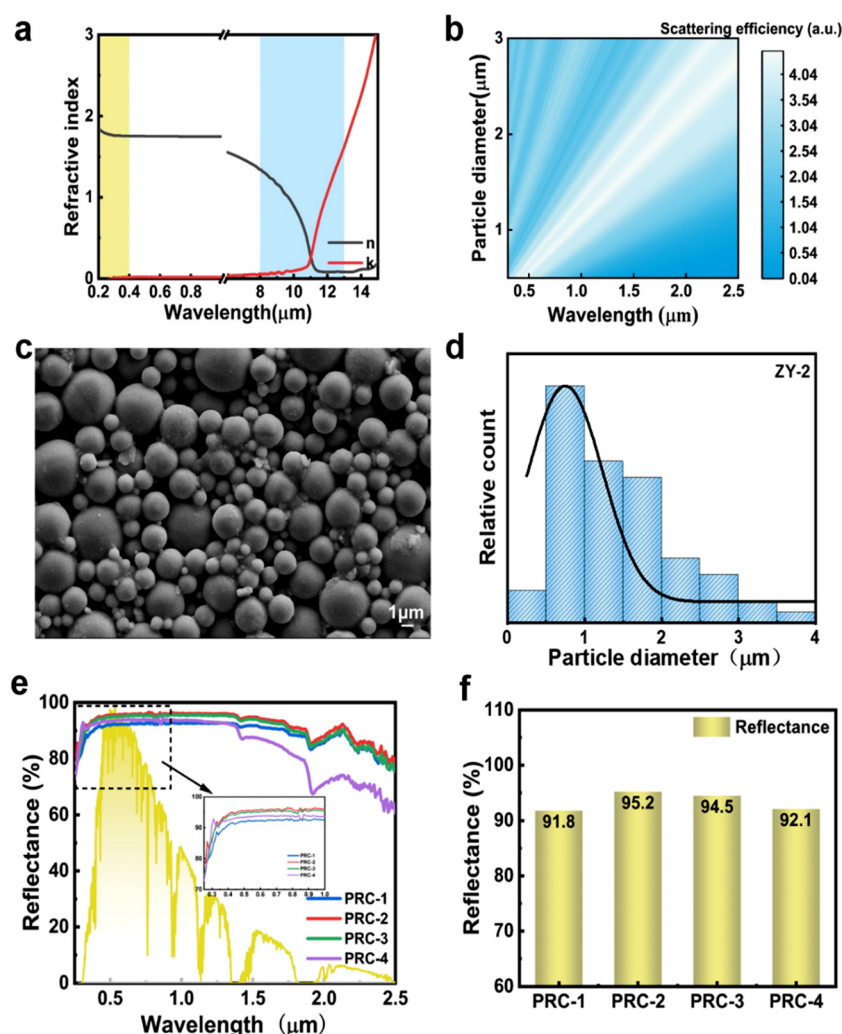

Fig. 2 Simulation and screening of Al_2O_3 particle size. (a) The complex spectral refractive index ($n + ik$) of Al_2O_3 in the solar and IR wavelength range (0–15 μm). (b) Simulated scattering efficiency of Al_2O_3 in the wavelength range of 0.25–2.5 μm with different diameters. (c) SEM images of ZY-2. (d) Particle diameter distribution of ZY-2. (e) UV-vis-NIR reflectance of PRC-1, PRC-2, PRC-3 and PRC-4. (f) The corresponding reflectance calculation values in Fig. 2e.

This journal is © The Royal Society of Chemistry 2025

J. Mater. Chem. C, 2025, **13**, 4137–4144 | **4139**

Paper

respectively, as calculated using eqn (S1) (ESI† (ref. 35)). The difference in particle size distribution of scatterers results in different spectra of the four coatings, among which ZY-4 has an excessively large average particle size, causing a significant decrease in the reflectance of PRC-4 in the near-infrared region (1.4–2.5 μm) and the reflectivity in the ultraviolet band is lower than that of other samples. The particle size distribution of ZY-2, mainly ranging from 0.5 to 3 microns, ensures strong scattering ability throughout the entire solar spectrum *via* Mie scattering. Consequently, PRC-2 exhibits the highest reflectivity, consistent with the simulation results. Furthermore, PRC-2 demonstrates high reflectivity in the ultraviolet band (more than 80%), indicating minimal ultraviolet absorption for both alumina and adhesive, thus suggesting excellent ultraviolet aging resistance for the coating. Based on these findings, ZY-2 is chosen as the scattering particle mixture.

3.2. Optimization of porosity

While the theoretical absorption of alumina in the solar spectrum is negligible, coatings unavoidably absorb solar energy due to impurities and defects. Hence, to minimize spurious absorption while maximizing the distance travelled by light inside the coating, the effect of porosity should be carefully investigated.

To this purpose, coatings with varying porosity were prepared by adjusting the powder-to-adhesive ratio (w:w) of 4:1, 3:2, 2:3, and 1:4, designated as PRC-2-4:1, PRC-2-3:2, PRC-2-2:3 and PRC-2-1:4. Fig. 3a illustrates the measured porosity of four coatings. Keeping the lowest amount of adhesive leads to the highest porosity about 40%, as confirmed *via* SEM pictures for the sample PRC-2-4:1 (Fig. S2, ESI†). The solar (0.25–2.5 μm)

reflectance of the four coatings was then tested and is depicted in Fig. 3b. It is observed that reflectance increases with increasing porosity, the R_s values of which are 94.6%, 87.3%, 80.8%, 70.7%, respectively (Fig. 3c).

To further clarify the influence of porosity on coating reflectivity, we calculate the average transport mean free path of photons in coatings with varying porosities.[36] By controlling the number of spray cycles to control the coating thickness, different thicknesses of coatings were obtained on a glass substrate. The transmittance of PRC-2-4:1 and PRC-2-2:3 was tested and fitted at a wavelength of 1064 nm. The results are shown in Fig. 3d and the average transport mean free path (l) of PRC-2-4:1 is about 4.4 μm, while that of PRC-2-2:3 is 14.7 μm, nearly 3.5 times greater than that of PRC-2-4:1. The average mean free path of the two coatings is consistent with the absorptivity calculated from Fig. 3d, showing that porosity affects the reflectivity of the coating by introducing more absorption-less scattering centres (air pores) and by increasing the refractive index contrast between the solid phase and air.

Furthermore, Fig. 3d illustrates that as the thickness reaches 0.4 mm, the transmittance decreases to 0.015. Subsequent increases in the coating thickness did not substantially increase the reflectance, suggesting that a 0.4 mm coating thickness is sufficient.

In the subsequent tests, the coating with an alumina-to-adhesive ratio of 4:1 and a spray thickness of 0.4 mm will be denoted as PRC-Al$_2$O$_3$.

3.3. Radiative cooling performance of the coating

To confirm the substrate independence of the coating optical properties, PRC-Al$_2$O$_3$ was applied to glass, aluminium, and
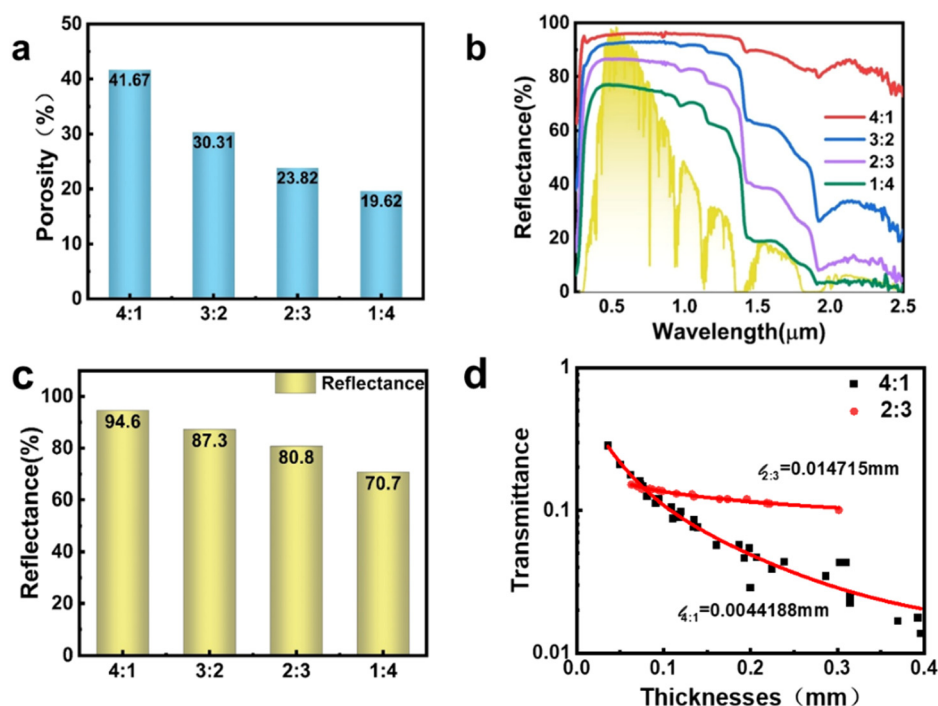

Fig. 3 (a) Porosity, (b) UV–vis–NIR reflectance of coating, and (c) the corresponding reflectance calculation values in Fig. 3b. (d) Different thickness with transmittance curve fitting and optical range calculation.

anodized aluminium plate (black) substrate, and their solar reflectance spectra (0.25–2.5 μm) are depicted in Fig. 4a, showing substantial overlap. The R_s values are 96.2%, 96.2%, and 96.1%, respectively. Similarly, as illustrated in Fig. 4b, the emissivity of PRC-Al_2O_3 on different substrates is nearly identical, measured at 92.1%, 92.1%, and 91.9%, respectively, thus verifying the substrate independence of PRC-Al_2O_3. The Si–O bond in sodium methylsilicate and the Al–O bond in alumina play a complementary role in enhancing the emissivity of the PRC-Al_2O_3 in the atmospheric window.

To highlight the advantages of PRC-Al_2O_3 coating, a commercial inorganic coating (CIC) with TiO_2 particles (XRD in Fig. S3, ESI†) as the scatterer was applied to an aluminium substrate. The spectra of CIC over solar (0.25–2.5 μm) and thermal infrared (2.5–25 μm) ranges are given in Fig. 4a and b. As expected, the reflection of the CIC sample in the UV range is lower due to the presence of TiO_2. Additionally, the reflection in IR range is also lower, which is probably due to the narrower particle size distribution that is typically concentrated at 0.2 μm to maximize visible reflectance. As a result, the R_s for the CIC is 85.5%, which is significantly lower than that of PRC-Al_2O_3. Combined with the similar emissivity of the two coatings, we expect the PRC-Al_2O_3 will exhibit a stronger radiation cooling performance.

To assess the daytime radiative cooling efficiency of PRC-Al_2O_3, we performed real-time temperature measurements on a clear day. The outdoor radiative cooling performance evaluation of the coating took place in Harbin, China. Fig. 5a depicts the apparatus designed for outdoor radiation cooling experiments, comprising a polyethylene film enclosing a polystyrene foam sample box to minimize and stabilize non-radiative heat exchange. Measurements were conducted under the weather conditions of July 9th, 2024 (Fig. 5b), with a relative humidity of 67% and an average wind speed of 2.6 m s^{-1}.

As shown in Fig. 5c, compared with the external air temperature, PRC-Al_2O_3 can achieve a continuous cooling effect through the day with respect to the external air temperature, despite the overheated air in the enclosed sample slot. Although CIC has a slight cooling effect inside the box, it does not have a cooling effect compared to the actual ambient temperature,[37] which can be attributed to its lower R_s (Fig. 4c).
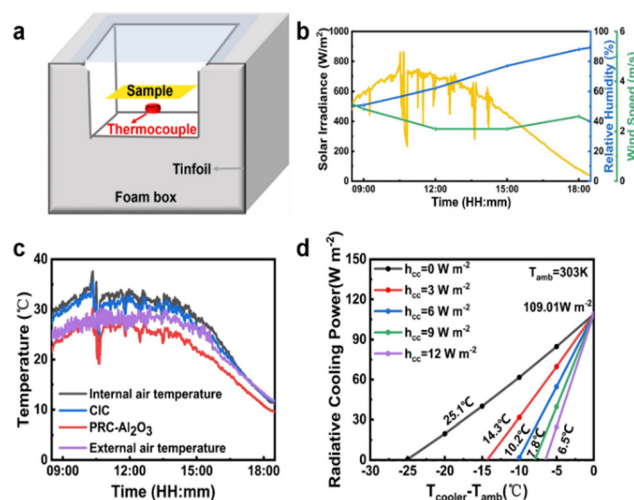

Fig. 5 Radiative cooling performances of coating. (a) Schematic diagram of outdoor temperature measurement device. (b) Solar irradiance, relative humidity, and wind speed data of the outdoor test environment (Harbin, 45°43′49″N, 126°38′11″E, China, July 9th 2024, 08:30–18:30). (c) Real-time temperature curves of the outdoor experiment with the PRC-Al_2O_3 and CIC (d) PRC-Al_2O_3 under different h_{cc} (0–12 W m^{-2}) at T_{amb} = 303 K during daytime.

The theoretical net radiative cooling capabilities of PRC-Al_2O_3 under direct sunlight were determined at various non-radiative heat transfer coefficients (h_{cc}) in comparison to conduction and convection, using equations outlined in Section S1.2 (ESI†) at a temperature of 303 K. With increasing h_{cc} values (0, 3, 6, 9, 12 W m^{-2} K^{-1}), the maximum temperature differences (ΔT) obtained are progressively reduced to 25.1 °C, 14.3 °C, 10.2 °C, 7.8 °C, and 6.5 °C, respectively (Fig. 5d). Additionally, we calculated the theoretical cooling power (P_{cool}) of the coating at different ambient temperatures (T_{amb}), illustrating how P_{cool} increases at higher T_{amb} in accordance with the blackbody radiation law (Fig. S4, ESI†).[38] The field test results confirm the promising cooling performance of our coating, even in humid regions.

3.4. UV durability and other properties of the coating

To assess the UV aging resistance of the coatings, PRC-Al_2O_3 and CIC were subjected together to UV irradiation for 72 hours. In Harbin, at an irradiation power of 0.7 kW m^{-2}, a 72-hour UV
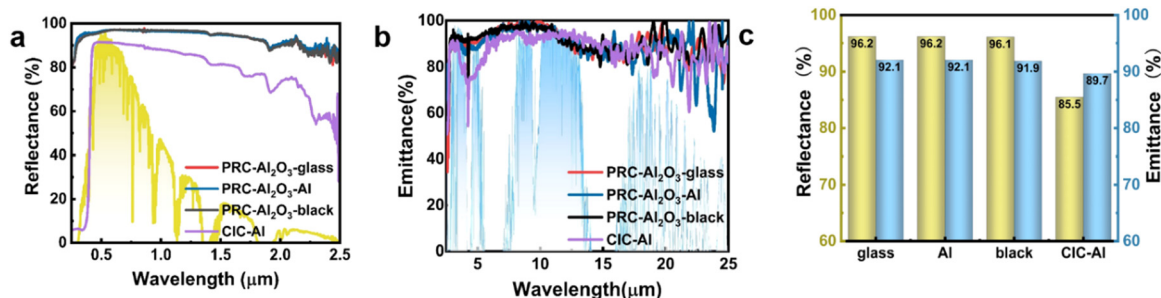

Fig. 4 Optical properties of the coatings. (a) UV-vis-NIR reflectance and (b) IR emittance of PRC-Al_2O_3 and CIC presented against the AM1.5 solar spectrum (yellow) and the atmospheric transparency window (blue), respectively. (c) The corresponding reflectance and emittance values in Fig. 4a and b.

exposure is equivalent to 48 days (Section S1.3, ESI†). As depicted in Fig. 6b, the reflectance of CIC significantly decreased in the wavelength range of 0.4–0.7 μm after 72 hours of UV aging, resulting in reductions in R_s of 5% (Fig. 6d). In contrast, PRC-Al$_2$O$_3$ exhibited minimal changes in the spectrum (Fig. 6a), indicating robust UV resistance. Additionally, the emittance of PRC-Al$_2$O$_3$ and CIC remained relatively unchanged (Fig. S5, ESI†). The UV aging resistance of PRC-Al$_2$O$_3$ is attributed to Al$_2$O$_3$ relatively wide bandgap (8.8 eV) compared to the energy of solar photons (0.49–4.13 eV), resulting in a significant increase in reflectivity in the solar spectrum.[39] In addition, the primary chain of methylated sodium silicate adhesive comprises Si–O bonds, with a binding energy (4.69 eV) which is also higher than the energy of solar photons, rendering them less prone to damage.[40] To demonstrate the durability of PRC-Al$_2$O$_3$ radiation cooling, the cooling performance of pristine and aged (accelerated UV aging, 72 h at 0.7 kW m^{-2}) samples was also tested outdoors on July 24th, 2024, with a relative humidity of 54% and an average wind speed of 1.9 m s^{-1} (Fig. S6, ESI†), showing that the coating maintains a comparable cooling effect to the unaged version, consistently with its minor decrease of solar reflectance.

In addition to UV radiation resistance, water resistance is also important for the actual service life of coatings. To this purpose, fluorinated coupling agents are frequently used to further improve the coating's hydrophobicity.[41] The optical properties and radiative cooling performance of the coating before and after modification remain basically unchanged (Fig. S6 and S7, ESI†); while the water contact angle of PRC-Al$_2$O$_3$ increased from 110° to 134°, the water contact angle of unmodified CIC was 76°, indicating a significant hydrophobic

effect of PRC-Al$_2$O$_3$. In addition, a roll-off angle of approximately 10° is observed for the hydrophobic PRC-Al$_2$O$_3$ coating (Video S1, ESI†). The changes in the surface water contact angle of the two coatings after UV aging for different durations are depicted in Fig. 6d. There was no significant decrease in the water contact angle after aging for PRC-Al$_2$O$_3$ and CIC, highlighting the advantages of inorganic coatings.

The adhesion between the coating and the substrate is crucial for the practical application of the coating. As depicted in Fig. S6 (ESI†), the coatings demonstrated excellent adhesion to the substrate, meeting level 0 standards. The pull-off method was employed to evaluate the bonding strength of our PRC-Al$_2$O$_3$ and CIC after exposure to UV radiation (Fig. S7, ESI†), indicating sustained good adhesion of the coating post-UV irradiation. In addition, the grid method is used to verify the adhesion of coatings soaked in acidic or alkaline solutions for 24 hours. The coatings exhibited strong adhesion to the substrate, meeting level 1 standards (Fig. S8, ESI†). These experimental results illustrate that even after 72 hours of UV irradiation or after soaking in acidic or alkaline solutions for 24 hours, the coating maintains good adhesion to the substrate, establishing a solid foundation for its future commercial use.

4. Conclusions

Alumina particles characterized by a wide bandgap and low absorption were selected to formulate coatings exhibiting substantial UV durability and radiative cooling performance, hence overcoming the typical limitations introduced by the use of more
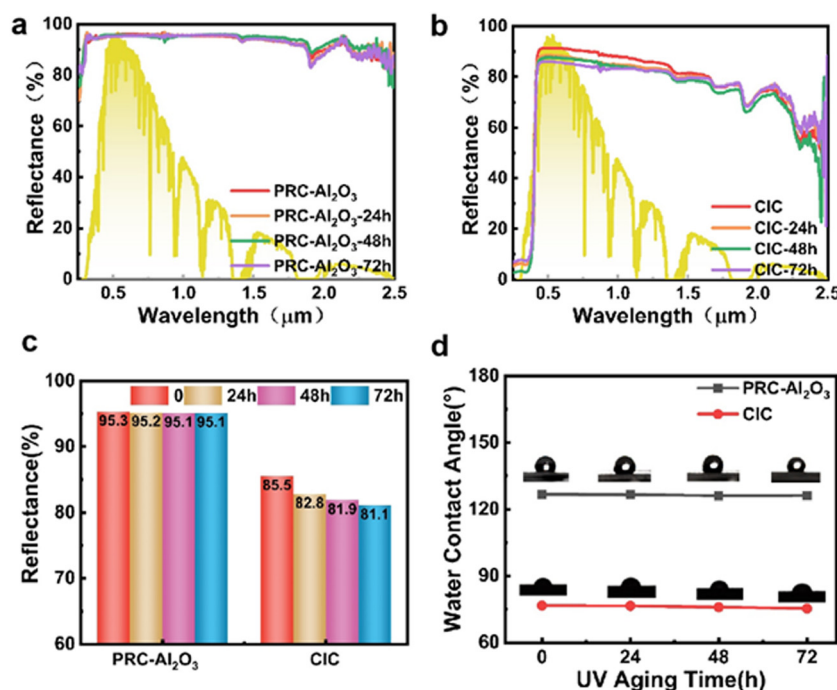

Fig. 6 The UV–vis–IR reflectance of (a) PRC–Al$_2$O$_3$ and (b) CIC before and after 72 h UV irradiation presented against the AM1.5 solar spectra (yellow), (c) calculated values of reflectance at different UV irradiation times. (d) Changes in the water contact angle before and after 72 h UV irradiation.

widely used inorganic nanoparticles with a higher refractive index. At a thickness of 0.4 mm, the coating demonstrates a solar reflectance of 96.2%, an infrared emissivity of 92.1%, achieving a maximum theoretical cooling power of 109 W m^{-2} and excellent resistance to weathering agents. Our results confirm that low refractive index scatterers can be utilized to formulate high reflectivity coatings using a fully inorganic paint formulation without the use of organic solvents, paving the way to the scalability required for commercial applications, and offering advantages in UV aging resistance. Aluminium oxide and sodium methylsilicate are affordable and readily available materials suitable for producing radiation cooling coatings on building roofs and exterior walls, providing a cost-effective solution to reduce associated overall costs.

Author contributions

Siyuan Li: investigation, data curation, formal analysis, visualization, writing – original draft; Xianglin Zhang: conceptualisation; Yanfei Yang: investigation; Xin Li: data curation, formal analysis; Hongbo Xu: conceptualisation, methodology, writing – review & editing; Juyan Zhao: writing – review & editing; Lorenzo Pattelli: conceptualisation, methodology, supervision, writing – review & editing; Lei Pan: conceptualisation, methodology, writing – review & editing; Jiupeng Zhao: supervision, writing – review & editing; Yao Li: supervision, writing – review & editing.

Data availability

Data supporting the results presented in this work are available in the ESI† and from the authors upon reasonable request.

Conflicts of interest

There are no conflicts to declare.

Acknowledgements

References

1 Q. Zhang, Z. Rao and R. Ma, Radiative cooling: arising from practice and in turn serving practice, *Nanophotonics*, 2024, **13**(5), 563–582, DOI: 10.1515/nanoph-2023-0678.

2 J. Liang, J. Wu and J. Guo, *et al.*, Radiative cooling for passive thermal management towards sustainable carbon neutrality, *Natl. Sci. Rev.*, 2023, **10**(1), nwac208, DOI: 10.1093/nsr/nwac208.

3 C. Hao, W. Cun-Hai and C. Zi-Ming, *et al.*, Performance analysis of thermoelectric system based on radiative cooling and greenhouse effects, *Acta Phys. Sin.*, 2021, **70**(21), 214401–214409, DOI: 10.7498/aps.70.20210356.

4 S. So, J. Yun and B. Ko, *et al.*, Radiative Cooling for Energy Sustainability: From Fundamentals to Fabrication Methods Toward Commercialization, *Adv. Sci.*, 2024, **11**(2), 2305067, DOI: 10.1002/advs.202305067.

5 M. Hossain and M. Gu, Radiative Cooling: Principles, Progress, and Potentials, *Adv. Sci.*, 2016, **3**(7), 1500360, DOI: 10.1002/advs.201500360.

6 Y. H. Chan, Y. Zhang and T. Tennakoon, *et al.*, Potential passive cooling methods based on radiation controls in buildings, *Energy Convers. Manage.*, 2022, **272**, 116342–116387, DOI: 10.1016/j.enconman.2022.116342.

7 B. Ziaeemehr, Z. Jandaghian and H. Ge, *et al.*, Increasing Solar Reflectivity of Building Envelope Materials to Mitigate Urban Heat Islands: State-of-the-Art Review, *Buildings*, 2023, **13**(11), 2868–2894, DOI: 10.3390/buildings13112868.

8 S. Feng, L. Yao and M. Feng, *et al.*, Sustainable regeneration of waste polystyrene foam as cooling coating: Building cooling energy saving, CO_2 emission reduction and cost-benefit prospective, *J. Cleaner Prod.*, 2024, **434**, DOI: 10.1016/j.jclepro.2023.140361.

9 F. L. Zhu and Q. Q. Feng, Recent advances in textile materials for personal radiative thermal management in indoor and outdoor environments, *Int. J. Therm. Sci.*, 2021, **165**, DOI: 10.1016/j.ijthermalsci.2021.106899.

10 Q. Jiang, Y. Wan and X. Li, *et al.*, Fabrication of thermal insulation sodium alginate/SiO_2 composite aerogel with superior radiative cooling function for firefighting clothing, *Pigm. Resin Technol.*, 2024, DOI: 10.1108/PRT-11-2023-0102.

11 Y. Zheng, Z. Fu and X. Sun, *et al.*, Al_2O_3/graphene/PVDF-HFP radiative cooling coating reinforced heat dissipation of BIPV modules, *J. Appl. Polym. Sci.*, 2024, DOI: 10.1002/app.55451.

12 C. Chen, B. Zhao and R. Wang, *et al.*, Janus Helical Ribbon Structure of Ordered Nanowire Films for Flexible Solar Thermoelectric Devices, *Adv. Mater.*, 2022, **34**(44), DOI: 10.1002/adma.202206364.

13 Y. Cui, X. Luo and F. Zhang, *et al.*, Progress of passive daytime radiative cooling technologies towards commercial applications, *Particuology*, 2022, **67**, 57–67, DOI: 10.1016/j.partic.2021.10.004.

14 P. Liu, Y. Sun and X. Huang, *et al.*, Colorful Superhydrophobic Composite Coating for Efficient Passive Radiation Cooling, *Ind. Eng. Chem. Res.*, 2023, **62**(51), 21995–22004, DOI: 10.1021/acs.iecr.3c03635.

15 H. Liu, F. Wang and S. Lei, *et al.*, Large-area fabrication of colorful superhydrophobic coatings with high solar reflectivity, *Constr. Build. Mater.*, 2021, **304**, 124602–124616, DOI: 10.1016/j.conbuildmat.2021.124602.

16 T. Du, J. Niu and L. Wang, *et al.*, Daytime Radiative Cooling Coating Based on the Y_2O_3/TiO_2 Microparticle-Embedded PDMS Polymer on Energy-Saving Buildings, *ACS Appl. Mater. Interfaces*, 2022, **14**(45), 51351–51360, DOI: 10.1021/acsami.2c15854.

17 A. L. Andrady, A. M. Heikkilae and K. K. Pandey, *et al.*, Effects of UV radiation on natural and synthetic materials,

This journal is © The Royal Society of Chemistry 2025

J. Mater. Chem. C, 2025, **13**, 4137–4144 | **4143**

Photochem. Photobiol. Sci., 2023, **22**(5), 1177–1202, DOI: **10.1007/s43630-023-00377-6**.

18 P. Li, Y. Liu and X. Liu, *et al.*, Reversed Yolk-Shell Dielectric Scatterers for Advanced Radiative Cooling, *Adv. Funct. Mater.*, 2024, **34**(23), DOI: **10.1002/adfm.202315658**.

19 J. Jung, S. Yoon and B. Kim, *et al.*, Development of High-Performance Flexible Radiative Cooling Film Using PDMS/TiO$_2$ Microparticles, *Micromachines*, 2023, **14**(12), 2223–2236, DOI: **10.3390/mi14122223**.

20 Z. Cheng, Y. Shuai and D. Gong, *et al.*, Optical properties and cooling performance analyses of single-layer radiative cooling coating with mixture of TiO$_2$ particles and SiO$_2$ particles, *Sci. China: Technol. Sci.*, 2021, **64**(5), 1017–1029, DOI: **10.1007/s11431-020-1586-9**.

21 A. Lamichhane, Energy-Gap-Refractive Index Relations in Semiconductors-Using Wemple-DiDomenico Model to Unify Moss, Ravindra, and Herve-Vandamme Relationships, *Solids*, 2023, **4**(4), 316–326, DOI: **10.3390/solids4040020**.

22 J. Mandal, Y. Yang and N. Yu, *et al.*, Paints as a Scalable and Effective Radiative Cooling Technology for Buildings, *Joule*, 2020, **4**(7), 1350–1356, DOI: **10.1016/j.joule.2020.04.010**.

23 R. Schaub, P. Thostrup and N. Lopez, *et al.*, Oxygen vacancies as active sites for water dissociation on rutile TiO$_2$ (110), *Phys. Rev. Lett.*, 2001, **87**(26), 266104, DOI: **10.1103/PhysRevLett.87.266104**.

24 J. Qiu, S. Li and E. Gray, *et al.*, Hydrogenation Synthesis of Blue TiO$_2$ for High-Performance Lithium-Ion Batteries, *J. Phys. Chem. C*, 2014, **118**(17), 8824–8830, DOI: **10.1021/jp501819p**.

25 Q. Wu, F. Huang and M. Zhao, *et al.*, Ultra-small yellow defective TiO$_2$ nanoparticles for co-catalyst free photocatalytic hydrogen production, *Nano Energy*, 2016, **24**, 63–71, DOI: **10.1016/j.nanoen.2016.04.004**.

26 X. Li, J. Peoples and P. Yao, *et al.*, Ultrawhite BaSO$_4$ Paints and Films for Remarkable Daytime Subambient Radiative Cooling, *ACS Appl. Mater. Interfaces*, 2021, **13**(18), 21733–21739, DOI: **10.1021/acsami.1c02368**.

27 X. Li, J. Peoples and Z. Huang, *et al.*, Full Daytime Subambient Radiative Cooling in Commercial-like Paints with High Figure of Merit, *Cell Rep. Phys. Sci.*, 2020, **1**(10), 100221, DOI: **10.1016/j.xcrp.2020.100221**.

28 Y. Zhai, Y. Ma and S. N. David, *et al.*, Scalable-manufactured randomized glass-polymer hybrid metamaterial for daytime radiative cooling, *Science*, 2017, **355**(6329), 1062–1066, DOI: **10.1126/science.aai7899**.

29 M.-T. Tsai, S.-W. Chang and Y.-J. Chen, *et al.*, Scalable, flame-resistant, superhydrophobic ceramic metafibers for sustainable all-day radiative cooling, *Nano Today*, 2023, **48**, 101745, DOI: **10.1016/j.nantod.2022.101745**.

30 K. Lin, S. Chen and Y. Zeng, *et al.*, Hierarchically structured passive radiative cooling ceramic with high solar reflectivity, *Science*, 2023, **382**(6671), 691–697, DOI: **10.1126/science.adi4725**.

31 X. Zhao, T. Li and H. Xie, *et al.*, A solution-processed radiative cooling glass, *Science*, 2023, **382**(6671), 684–691, DOI: **10.1126/science.adi2224**.

32 T. Li, H. Sun and M. Yang, *et al.*, All-Ceramic, compressible and scalable nanofibrous aerogels for subambient daytime radiative cooling, *Chem. Eng. J.*, 2023, **452**, 139518, DOI: **10.1016/j.cej.2022.139518**.

33 M. Burresi, L. Cortese and L. Pattelli, *et al.*, Bright-White Beetle Scales Optimise Multiple Scattering of Light, *Sci. Rep.*, 2014, **4**(1), 6075–6083, DOI: **10.1038/srep06075**.

34 Q. Yue, L. Zhang and C.-Y. He, *et al.*, Polymer composites with hierarchical architecture and dielectric particles for efficient daytime subambient radiative cooling, *J. Mater. Chem. A*, 2023, **11**(6), 3126–3135, DOI: **10.1039/D2TA07453B**.

35 X. Li, L. Pattelli and Z. Ding, *et al.*, A Novel BST@TPU Membrane with Superior UV Durability for Highly Efficient Daytime Radiative Cooling, *Adv. Funct. Mater.*, 2024, DOI: **10.1002/adfm.202315315**.

36 A. I. Shestakov, Multifrequency radiation diffusion equations for homogeneous, refractive, lossy media and their interface conditions, *J. Comput. Phys.*, 2013, **243**, 293–304, DOI: **10.1016/j.jcp.2013.03.016**.

37 G. E. Lio, J. Werlé and M. Arduini, *et al.*, Radiative Cooling Potential of a Water-Based Paint Formulation under Realistic Application Conditions, *ACS Appl. Opt. Mater.*, 2024, DOI: **10.1021/acsaom.4c00099**.

38 J. Song, W. Zhang and Z. Sun, *et al.*, Durable radiative cooling against environmental aging, *Nat. Commun.*, 2022, **13**(1), 4805–4817, DOI: **10.1038/s41467-022-32409-7**.

39 L. Hu, A. Narayanaswamy and X. Chen, *et al.*, Near-field thermal radiation between two closely spaced glass plates exceeding Planck's blackbody radiation law, *Appl. Phys. Lett.*, 2008, **92**(13), 133106–133110, DOI: **10.1063/1.2905286**.

40 D. Chae, S. Son and H. Lim, *et al.*, Scalable and paint-format microparticle–polymer composite enabling high-performance daytime radiative cooling, *Mater. Today Phys.*, 2021, **18**, 100389–100398, DOI: **10.1016/j.mtphys.2021.100389**.

41 X. Yang, J. Geng and R. Xu, *et al.*, Self-cleaning energy-free PDMS@KL film for daytime radiative cooling, *Mater. Lett.*, 2023, **350**, 134831–134835, DOI: **10.1016/j.matlet.2023.134831**.